An Interface-Induced Co-Assembly Approach Towards Ordered Mesoporous Carbon/Graphene Aerogel for High-Performance Supercapacitors

Ruili Liu, Li Wan, Shaoqing Liu, Lixia Pan, Dongqing Wu,* and Dongyuan Zhao*

Hierarchically porous composites with mesoporous carbon wrapping around the macroporous graphene aerogel can combine the advantages of both components and are expected to show excellent performance in electrochemical energy devices. However, the fabrication of such composites is challenging due to the lack of an effective strategy to control the porosity of the mesostructured carbon layers. Here an interface-induced co-assembly approach towards hierarchically mesoporous carbon/graphene aerogel composites, possessing interconnected macroporous graphene networks covered by highly ordered mesoporous carbon with a diameter of ≈9.6 nm, is reported. And the orientation of the mesopores (vertical or horizontal to the surface of the composites) can be tuned by the ratio of the components. As the electrodes in supercapacitors, the resulting composites demonstrate outstanding electrochemical performances. More importantly, the synthesis strategy provides an ideal platform for hierarchically porous graphene composites with potential for energy storage and conversion applications.

1. Introduction

Graphene aerogel (GA) has recently become an intensively studied subject since its macroporous architecture can shift the intriguing properties of graphene sheets including high electrical conductivity and good mechanical stability into a three-dimensional (3D) interconnected framework and thus actualize the exciting applications of graphene in biology, catalysis, energy conversion and storage.[1] To enhance their physical properties or introduce new capabilities, GA can also serve as the monolithic substrates for the loading of various nanomaterials including metal oxides,[2] silicas,[2f,3] polymers[4] and even carbons.[2f,3b,5] The synergistic effects of GA and the additional components enable the resultant GA composites to delivery much enhanced electrochemical performance in diversified energy devices such as lithium ion batteries,[2a,3b] supercapacitors[2f,4a,b,5a,b] and fuel cells.[2d,5c,d,6]

With the advantages of highly ordered pores, large surface area and high physisorption capacity, ordered mesoporous carbon (OMC) has received intensive attention from material scientists for decades.[7] Nevertheless, the low crystalline degree and large amount of defects in the framework of OMC inevitably retard the electron transfer and weaken their electrochemical activity.[7d,8] The combination of OMC with GA will generate the composites with uniform mesoporous carbon layers coating on the highly conductive 3D graphene backbone, which are expected to greatly facilitate their electrochemical applications.[2f] However, such hierarchically porous composites have not been reported so far, mainly due to the lack of an effective synthesis method to control the porosity of the mesoporous carbon layers on the surface of GAs.

When graphene oxide (GO) is used as the building block for GA,[1g,9] the residue oxygen containing groups endow GA with amphiphilic pore walls, which can absorb the micelles of surfactants via non-covalent forces such as hydrophilic and ionic interactions.[2f,3] It should be noted that the utilization of the surfactant micelles as the soft-templates for ordered mesoporous materials have been well-developed.[7a,10] With these soft-template methods, the fabrication of porous materials with tunable porosities on diversified substrates has also been reported by several research groups.[3b,5a,b,d,11] Inspired by these results, we envision that the fabrication of OMC on GA will be experimentally feasible by the selection of proper surfactants, carbon sources as well as synthetic methods.

Herein, we report for the first time a fabrication strategy towards the composites of ordered mesoporous carbon and graphene aerogel (OMC/GA) *via* an interface-induced co-assembly process and the following carbonization, in which GA is used as a macroporous substrate, triblock copolymer F127 as a soft template and resols as carbon sources. The resultant OMC/GAs possess interconnected macroporous graphene networks covered by OMC with a uniform pore size

Prof. R. L. Liu, L. Wan, S. Q. Liu, L. X. Pan
Department of Chemical Engineering
School of Environment and Chemical Engineering
Shanghai University
Shangda Road 99, Shanghai 200444, P. R. China
E-mail: ruililiu@shu.edu.cn
Prof. D. Q. Wu
School of Chemistry and Chemical Engineering
Shanghai Jiao Tong University
Dongchuan Road 800, Shanghai 200240, P. R. China
E-mail: wudongqing@sjtu.edu.cn
Prof. D. Y. Zhao
Laboratory of Advanced Materials
Department of Chemistry and Shanghai Key Laboratory of Molecular Catalysis and Innovative Materials, Fudan University
Shanghai 200433, P. R. China

DOI: 10.1002/adfm.201403280

of 9.6 nm. And the orientation of the mesopores (vertical or horizontal to the surface of GA) can be easily modified by the ratio of the components in the co-assembly process, which also demonstrates strong influence on the electrochemical behavior of OMC/GAs serving as the electrodes in supercapacitors. The all-solid-state supercapacitor (ASSS) based on OMC/GA with vertical mesopores exhibits an outstanding specific capacitance (44.3 F g^{-1}) at 5 mV s^{-1}, excellent cycling stability (7.4% loss after 1000 cycles), and high power density at fast charge/discharge process (≈3545 Wh Kg^{-1} at less 3.6 s). Compared with the routes reported previously, our soft-template approach provides a more facile, economic and controllable solution towards hierarchically porous graphene composites.

2. Results and Discussion

2.1. Fabrication of OMC/GA Composites with Controllable Mesostructures

A series of OMC/GAs were prepared by adjusting the mass ratio (*R*) of resol-F127 monomicelles to GA, denoted as OMC/GA-1 (*R* = 2.5), OMC/GA-2 (*R* = 6), OMC/GA-3 (*R* = 10) and OMC/GA-4 (*R* = 15), respectively. In controlled experiments, pristine GA[9] as well as OMC[12] were also prepared (See details in Experimental Section).

The morphology and microstructure of OMC/GAs were first characterized by scanning electron microscopy (SEM) and transmission electron microscopy (TEM). SEM images show that OMC/GA-2 has a highly interconnected 3D framework containing macropores with the diameters ranging from 3 to 8 μm (Figure S1a, Supporting Information). Such macroporous monolithic architectures are still retained (**Figure 1**a,b) even after the assembly of the mesoporous carbon, indicating that the resol-F127 monomicelles and carbon layers derived from them are successfully bound on the wall surface of GA without destroying the 3D framework. The high-resolution SEM (HRSEM) images further confirm that the graphene sheets are covered with mesoporous carbon (Figure 1c–e). More importantly, the morphology and the thickness of mesoporous carbon in OMC/GA composites exhibit obvious dependence on the amount of resol-F127 monomicelles. With the lowest mass ratio of resol-F127 to GA, the surface of OMC/GA-1 is sparsely decorated by porous carbon with irregular domains (Figure S2a, Supporting Information). In contrast, the macropore walls of OMC/GA-2 with a thickness of ≈10 nm are homogeneously sandwiched by mesoporous carbon layers (Figure 1c and Supporting Information Figure S1b), suggesting that the quantity of the monomicelles is enough to enwrap the graphene scaffold of GA.

It is interesting that mesoporous carbon arrays in the composite OMC/GA-2 are vertically grown on the underlying graphene sheets in an ordered hexagonal pattern. TEM images (**Figure 2**a,b) further verify that the graphene sheets are coated by carbon layers containing perpendicularly aligned mesopores with a diameter of ≈9.6 nm and a wall-thickness of ≈4 nm. These mesopores should be originated from the thermal decomposition of F127 since the sizes match with the reported diameter of the micelles from the triblock copolymer.[11a] Impressively, the incremental mass ratio of the resol-F127 monomicelles in OMC/GA-3 leads to the increased wall-thickness of ≈12 nm (Figure S1c, Supporting Information) and

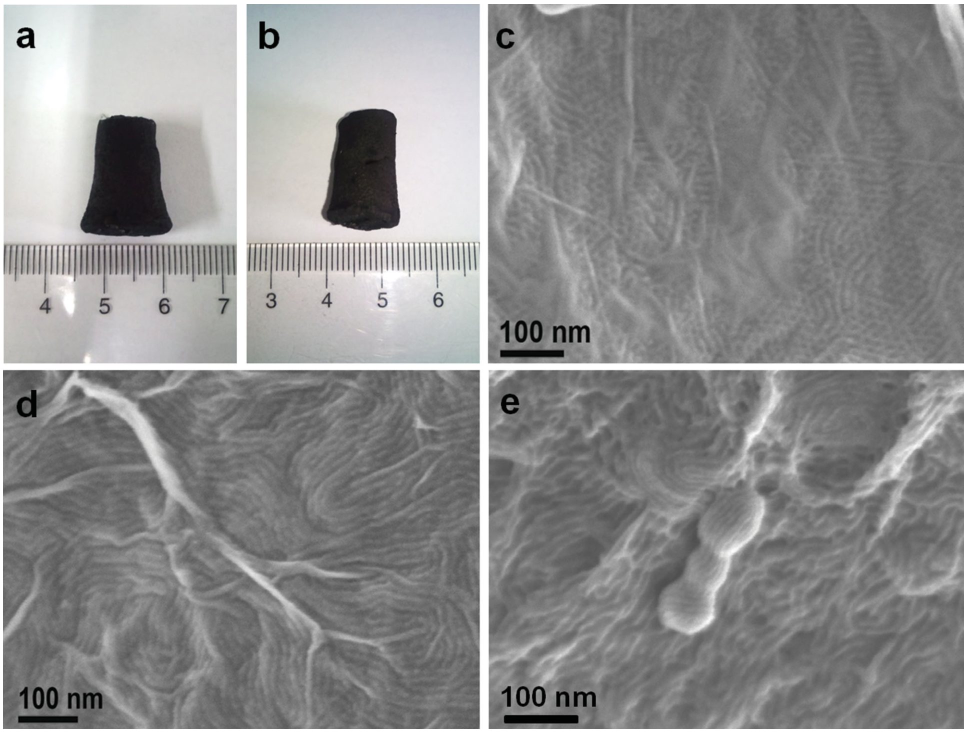

Figure 1. Morphology and structure of OMC/GA composites. Digital images of as-made OMC/GA-2 obtained a) after hydrothermal self-assembly and b) after thermal treatment at 700 °C in N_2. High-resolution SEM images of c) OMC/GA-2, d) OMC/GA-3, and e) OMC/GA-4.

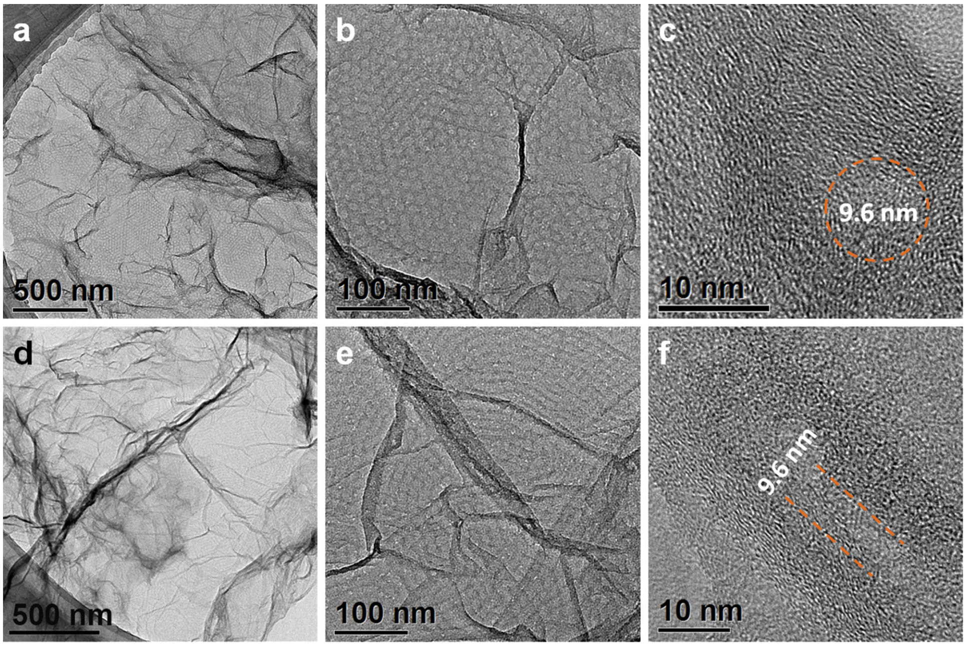

Figure 2. TEM images of OMC/GAs. a,b) Low- and c) high-resolution TEM images of OMC/GA-2. d,e) Low- and f) high-resolution TEM images of OMC/GA-3.

the formation of carbon layers with uniform channel-shaped mesopores on the graphene surface (Figure 1d, 2d,e). Similar to the vertically aligned mesopores in OMC/GA-2, the diameters of the fingerprint-like mesopores OMC/GA-3 are also measured to be ≈9.6 nm. In comparison, OMC/GA-4 with the highest added amount of the monomicelles isn't only covered by the carbon layers with meso-sized grooves, but also decorated by mesoporous carbon spheres with a diameter of about 100 nm (Figure 1e, and Supporting Information Figure S1d,S2b).

Furthermore, as illustrated in the HRTEM images of OMC/GA-2 (Figure 2c) and OMC/GA-3 (Figure 2f), the well-resolved lattice fringes aligned around the mesopores disclose the high crystallinity degree of their mesoporous carbon layers. The highly graphitic degree of OMC/GA composites is further confirmed by the X-ray diffraction (XRD) and Raman spectroscopy. All the samples exhibit similar XRD patterns, and the major diffraction peak around 26.0° can be indexed to the (002) diffraction plane of graphite (Figure S3a, Supporting Information). In the Raman spectra, two broad peaks around 1330 and 1593 cm^{-1} are assigned to the D and G band of carbon, respectively (Figure S3b, Supporting Information).[11a] Among them, the G band of OMC/GA-2 is distinctly sharper than that of GA, and the intensity ratio of G to D band (I_G/I_D) increases from 1.1 (GA) to 1.5 (OMC/GA-2).

The porosity of OMC/GAs was further characterized by N_2 adsorption measurements. In their N_2 adsorption/desorption isotherms, all the samples show a typical type IV curve with a combination of H2 and H4 hysteresis loop at relative pressures (P/P_0) of 0.45–1.0 (Figure S4, Supporting Information), indicating the existence of mesopores in platelet-like structures.[13] Brunauer-Emmett-Teller (BET) analysis reveals that the range of the specific surface areas and pore volumes for OMC/GAs are 248–265 $m^2\ g^{-1}$ and 0.45–0.51 $cm^3\ g^{-1}$, respectively (**Table 1**), which are comparable to the mesoporous carbon/GA composites derived from the hard-template route[3b] and mesoporous graphene nanosheets.[11a]

2.2. Electrochemical Characterization

The combination of hierarchically porous structure with highly oriented mesopores, 3D graphitic framework and high ion-accessible surface area makes the OMC/GA composites extremely desirable for high power and long cycle life electrochemical capacitors. To evaluate the electrochemical behavior of OMC/GAs, cyclic voltammetry (CV) and galvanostatic charge-discharge measurement were employed in a three-electrode system with 6.0 M aqueous KOH as the electrolyte at potential interval from –1.0 to 0 V versus Hg/HgO electrode. For

Table 1. Porosity and electrochemical performance of OMC/GAs, GA, and OMC.

Sample	$R^{a)}$	$D^{b)}$ [nm]	$S_{BET}{}^{c)}$ [$m^2\ g^{-1}$]	$V^{d)}$ [$cm^3\ g^{-1}$]	$C^{e)}$ [$F\ g^{-1}$]	$C_{device}{}^{f)}$ [$F\ g^{-1}$]
GAs	0	6.9	220	0.45	130	35.6
OMC/GA-2	6	9.6	254	0.49	197	44.3
OMC/GA-3	10	9.6	265	0.51	166	37.7
OMC/GA-4	15	9.6	248	0.45	133	42.4
OMC	∞	2.6	1030	1.30	123	31.9

[a)] R is the mass ratio of F127/resol monomicelles to GA; [b)] D is the pore size diameter; [c)] S_{BET} is the BET surface area; [d)] V is the total pore volume; [e)] C was calculated from the galvanostatic discharge in three-electrode system at the current density of 0.5 A g^{-1}; [f)] C_{device} was calculated from the cyclic voltammetry based on two-electrode mass of active materials at the scan rate of 5 mV s^{-1}.

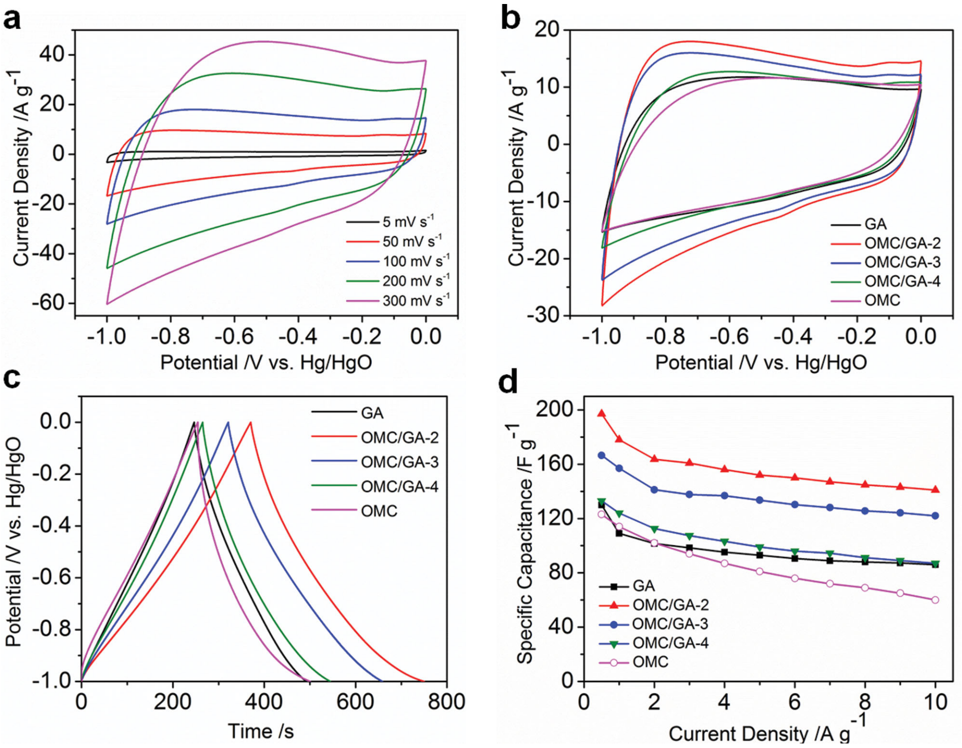

Figure 3. Comparison of OMC/GAs, GA and OMC in a three-electrode system with 6 M KOH as the electrolyte. a) CV curves of OMC/GA-2 at different scan rates. b) CV curves of the samples obtained at 100 mV s^{-1}. c) Galvanostatic charge-discharge curves measured at a current density of 0.5 A g^{-1}. d) Specific capacitance retention of the samples with varied current densities.

comparison, pure GA and OMC electrodes were also tested under the same conditions.

As indicated by **Figure 3**a and S5, all the samples exhibit the increment in the area of the CV with the increase of the sweep rates. Moreover, it can be discerned that OMC/GA-2 and OMC/GA-3 reveal a larger capacitive response than OMC/GA-4, pure GA and OMC. Also, their CV curves show nearly symmetrical rectangular shapes and maintain well even at the scan rate up to 300 mV s^{-1}, indicative of an ideal capacitive behavior (Figure 3b). This point is further confirmed by their quasi triangular-shaped galvanostatic charge/discharge cycling curves (Figure 3c). Specifically, the capacitance of OMC/GA-2 is about 197 F g^{-1} at a current density of 0.5 A g^{-1}, higher than those of GA (130 F g^{-1}), OMC (123 F g^{-1}) and OMC/GA-3 (166 F g^{-1}). In order to investigate the capacitance retention of OMC/GA electrodes at high current density, the variation of specific capacitance at different current densities are summarized in Figure 3d. Notably, OMC/GA-2 exhibits a high rate capability of 141 F g^{-1} at a current density as high as 10 A g^{-1}. Not just superior to the other samples in this work, the excellent electrochemical performance of OMC/GA-2 including substantially large capacity and high rate capability also overruns the conventional mesoporous carbon,[14] pure graphene,[2f,9,15] nitrogen/boron co-doped GA,[16] and resol-derived carbon/GA composites.[17]

Given the remarkable electrochemical performance, ASSSs with OMC/GAs as electrode materials and polyvinyl alcohol (PVA)/H_2SO_4 gel as a solid-state electrolyte were assembled in this work (Figure S6, Supporting Information). In the ASSSs, the CV curves of OMC/GA-2 and OMC/GA-3 still keep the rectangular symmetry at different scan rates between 0 and 1 V, even at a scan rate as high as 300 mV s^{-1} (**Figure 4**a and Supporting Information Figure S7). Similar to the results from the three electrode measurements, the ASSS with OMC/GA-2 as electrode deliveries the highest specific capacitance (44.3 F g^{-1} at a scan rate of 5 mV s^{-1}), rate capability (23.6 F g^{-1} at 300 mV s^{-1}) and cycling stability (retaining ≈92.6% of the initial capacitance after 1000 cycles), outperforming the other OMC/GAs (Figure 4b,c and Table 1). Calculated by integrating the CV curves at different scan rates based on the Ragone plot (Figure 4d), the ASSS from OMC/GA-2 also manifests the highest energy density (≈6.2 W h Kg^{-1} at 5 mV s^{-1}) and power density (≈3545 W Kg^{-1} at less than 3.6 s) among all the samples in this work (Table 1). Moreover, the exceptional power density of the ASSS with OMC/GA-2 as electrode is over twice higher than that of capacitor based on the nitrogen/boron doped GAs.[16]

2.3. Discussion

On the basis of the above structural characterization, the formation mechanism of OMC/GAs is proposed as an interface-induced co-assembly pathway of resol-F127 monomicelles with GA (**Figure 5**). Firstly, the as-prepared phenolic resols are assembled with Pluronic triblock copolymer into spherical monomicelles as subunit building blocks.[12] When these monomicelles are mixed with GA, they can gradually deposit

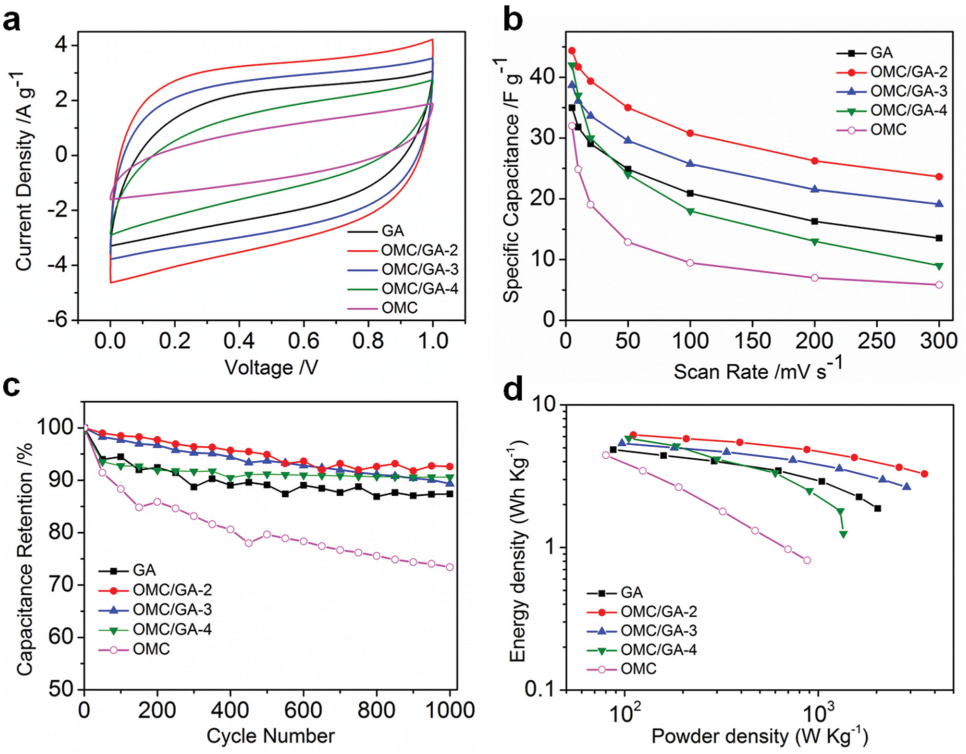

Figure 4. Comparison of ASSSs based on OMC/GAs, GA and OMC. a) CV curves obtained at the scan rate of 100 mV s^{-1}. b) Specific capacitance retention as a function of scan rates from 5 to 300 mV s^{-1}. c) Cycling stability obtained from CV curves at 50 mV s^{-1} for 1000 circles and the specific capacitance is calculated after each 100 circles. d) Ragone plot of the ASSSs, based on the mass of active materials.

on the macrospore walls of GA via strong non-covalent forces such as hydrogen-bonds, amphiphilic interactions and π–π interactions since both monomicelles and GA contain plenty of oxygen rich groups and aromatic units.[2b,18] It is worthy to note that the wall-thicknesses of OMC/GA-2 and OMC/GA-3 do not exceed the diameters of two resol-F127 monomicelles,[12] implying that the graphene sheets in GA are sandwiched by one single layer of the monomicelles on each side during the co-assembly process. Obviously, the formation of a flat layer of the monomicelles on the surface of GAs via heterogeneous nucleation (OMC/GA-2 and OMC/GA-3) is more favorable than the 3D aggregation of the monomicelles *via* homogeneous nucleation (OMC/GA-4 with carbon spheres were generated by heteraogeneous and homogeneous nucleation process), thus indicating that the non-covalent forces between the monomicelles and GA are stronger than the interactions among the monomicelles. During the interface-induced deposition process, these monomicelles are continuously deposited, assembled, and then slowly transformed into an ordered array by a close packing route to form the lowest energy state. Interestingly, the distinct morphologies of OMC/GA-2 and OMC/GA-3 imply that the assembly of monomicelles on GA is highly concentration-dependent. When the mass ratio of the monomicelles to GA is relatively low (R = 6.0 in OMC/GA-2), the monomicelles prefer to keep their spherical morphology and form hexagonal arrays on the surface GA.[11a] With the increasing of their concentration (R = 10 in OMC/GA-3), the resol-F127 monomicelles can reform into terrace-like aggregates, which thus allow for the accommodation of more monomicelles on the surface of GA. Under the hydrothermal

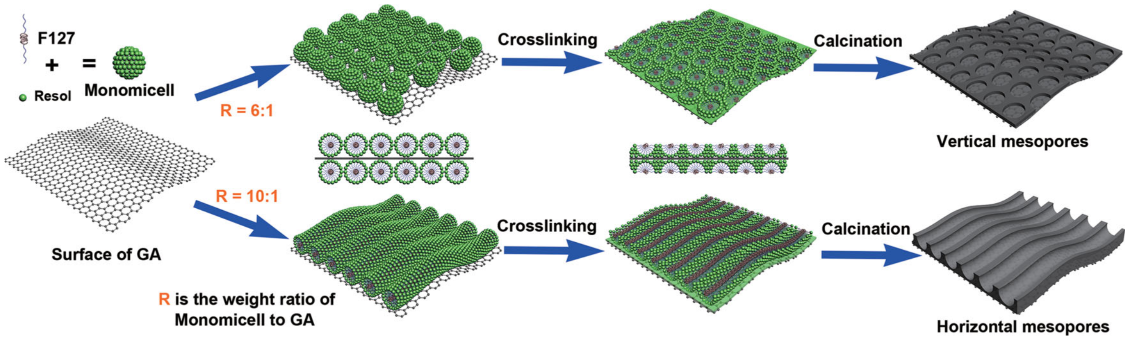

Figure 5. Schematic illustration of the formation process for OMC on GA.

conditions, these monomicelles are solidified into cross-linked polymer layers and the different arrangements of the monomicelles result in different mesopores (vertical or horizontal to the surface of GA) in this process. The carbonization of mesoporous polymers to graphitic carbon and the reduction of GA can happen simultaneously at the following high temperature calcinations, which subsequently lead to OMC/GA composites with different mesoporosity.

In both the three-electrode system and the ASSSs, OMC/GA-2 and OMC/GA-3 surpass either OMC or GA at all the tested charging rates, which is unambiguously owing to the synergistic effects of OMC and GA in the composites. Firstly, the poor rate capability and cycling stability of the OMC based electrodes clearly testify the importance and necessity of the highly conductive graphene framework in the OMC/GA composites. Secondly, it seems that the morphology of OMC in the composites also has influence on their electrochemical performance in supercapacitors. Lacking of ordered mesoporous structures, resol-derived carbon/GA composites with much higher surface areas[17] still cannot deliver a better specific capacitance than OMC/GAs, indicating the importance of the micelle-templated mesostructure. Moreover, OMC/GA-2 with vertically oriented mesopores manifests higher capacitance and rate performance than OMC/GA-3 with horizontal aligned mesopores although they have similar surface areas, pore volumes and pore size distributions. The differences in the electrochemical behaviors of OMC/GA-2, OMC/GA-3 and OMC/GA-4 may also be attributed to the varied weight content of OMC in the composites. Typically, OMC/GA-4 with high content of OMC shows fast decay with the increase of scan rates although it has similar surface area and mesoporous structure to OMC/GA-3 (Figure 3d, 4c). This may be attributed to the existence of the mesoporous carbon spheres in OMC/GA-4, which lead to higher electrochemical resistance than that of graphene in solid state electrolyte. To validate the hypothesis, the electrochemical impedance spectra (EIS) of OMC/GAs and GA were further measured and compared (Figure S8, Supporting Information). Nyquist plots features a vertical curve in OMC/GA-2 electrode at the low frequency region, which is characteristic of a pronounced capacitive behavior. At high-frequency region, a transition from a vertical curve feature to a –50° line followed by a semicircle is observed as the increment of OMC in the composites, suggesting the increased contact and charge-transfer resistances. The absence of a loop in the impedance spectra of OMC/GA-2 indicates that OMC layer enhance the electronic conductivity between GAs and current collector.[20] Moreover, the resistance of OMC/GA-2 is even lower than GA without involving OMC, which is presumably owing to the carbon at the joints of the graphene sheets facilitating the electron transport within the 3D framework of the composites.[1e,19] The successful combination of uniform porous structures and high electrical conductivity in OMC/GA-2 explains its excellent capacitance, rate capability and stability as the electrode materials in supercapacitors.

3. Conclusion

This work demonstrates an unprecedented interface-induced co-assembly route to fabricate the monolithic composites of OMC and GA, in which the interconnected graphene scaffolds are uniformly wrapped by OMC with highly oriented mesopore arrays. The mesostructures of the resultant OMC/GAs can be facilely modified by adjusting the mass ratio of the components during the assembly process, which further influence the electrochemical behaviors of the composites. As the electrodes in supercapacitors, OMC/GAs delivered prominent performance including high capacitance, rate capability and energy/power density. More importantly, our approach provides an intriguing platform towards various hierarchically porous graphene composites with controllable meso-scaled porosity, which is expected to have a broad range of applications in electrochemical capacitor, batteries, sensors, and catalysis.

4. Experimental Section

Synthesis of OMC/GAs: First, GO was prepared from natural graphite powder using a modified Hummers method.[21] Subsequently, GA with macroporosity and good mechanical stability was produced from the hydrothermal assembly of GO in an aqueous suspension (1.5 mg mL^{-1}) under 180 °C for 12 h and the following freeze-drying process.[9] On the other hand, spherical resol-F127 monomicelles were synthesized by organic-organic self-assembly of resol molecules with triblock copolymer Pluronic F127.[11a,12] In a typical synthesis, phenol (0.60 g) was melted at 40 °C and NaOH aqueous solution (0.1 M, 15 mL) was added slowly to the round-bottom flask with continuous stirring. Then an aqueous solution of formaldehyde (37 wt%, 2.1 mL) was added dropwisely and the reaction mixture was stirred at 70 °C for 0.5 h to obtain low-molecular-weight phenolic resols. After that, an aqueous solution of F127 (6 wt%, 15 mL) was added, and the resulting mixture was stirred at 70 °C for another 2 hours. Subsequently, H_2O (50 mL) was added to dilute the solution and further stirred at 67–70 °C for over 12 h until the color of the solution turned to crimson. To fabricate OMC/GA composites, a certain amount of the as-prepared resol-F127 monomicelles solution (5, 12, 20, and 30 mL) was dilute to 73 mL with Milli-Q water and transferred into a Teflon lined stainless steel autoclave (100 mL). GAs were then immersed into the aqueous solution of monomicelles and kept still for 12 h for sufficient contact between GAs and monomicelles. Afterword, the mixture was hydrothermally treated at 130 °C for 20 h. After cooled to room temperature, the resulting monolith was washed with water and dried at 40 °C for 2 days, followed by carbonization at 700 °C in nitrogen to produce OMC/GA composites. According to the different amount of resol-F127 monomicelles, the products were named as OMC/GA-1 (5 mL), OMC/GA-2 (12 mL), OMC/GA-3 (20 mL) and OMC/GA-4 (30 mL). In control experiments, GA monolith[9] and OMC[12] derived from the self-assembly of spherical phenolic resol-F127 monomicelles without GA were also thermally treated at 700 °C in nitrogen and the resultant products were collected for the following structural characterization and property measurement.

Characterization: X-ray diffraction (XRD) patterns were recorded on a Rigaku D/MAX 2200V/PC X-ray diffractometer using Cu Kα radiation (40 kV, 20 mA). Transmission electron microscopy (TEM) measurements were conducted on a JEM-2010F (JEOL, Japan) operated at 200 kV. Samples were suspended in ethanol and transferred onto a Cu grid for TEM measurements. Field emission-scanning electron microscopy (FE-SEM) images were taken on a JSM-7401F (JEOL Ltd., Japan) microscope. Raman spectra were recorded with Brucker RFS 100/S spectrometer. Nitrogen sorption isotherms were measured at 77 K with an Autosorb-1MP instrument (Quantachrome, USA). Before measurements, the samples were degassed in a vacuum at 200 °C for at least 12 h.

Electrochemical Measurement: Electrochemical measurements were carried out using a CHI 660E electrochemical workstation under ambient condition. In a three-electrode system, 6 M KOH was used as the aqueous electrolyte, a platinum plate as the counter electrode, and a Hg/HgO electrode as the reference electrode. To prepare the working electrode, a homogeneous slurry containing polytetrafluoethylene (PTFE, 1 wt%) and active materials (weight ratio 1:9, in ethanol) was painted between two pieces of nickel foam with area of 1 cm^2 and pressed under 15 MPa face to face for 5 min. The electrode was then dried at 100 °C in vacuum overnight. The mass loading of the active material was calculated by the mass difference of the nickel foams before and after the loading of active materials. In the case of all-solid-state supercapacitors (ASSSs),[16,22] gel-like electrolyte was first fabricated by mixing H_2SO_4 (6 g) and PVA (6 g) in deionized water (60 mL) and thus heated up to 80 °C under vigorous stirring until the solution becomes clear. Two slices of platinum plate were painted with the active material on each plate, and then immersed in the PVA/H_2SO_4 electrolyte at 80 °C for 5 min. The resulting electrolyte-filled electrodes were solidified for 12 h at room temperature. Finally, as-prepared two electrodes were symmetrically face to face integrated into one ASSS under a pressure of about 5 MPa for 5 min.

Calculations: The electrochemical performance of the OMC/GA electrode in KOH (6 M) was examined by cyclic voltammetry (CV) and galvanostatic charge-discharge. The single electrode capacitance was calculated from the galvanostatic discharge process according to the following equation:

$$C = \frac{I \times \Delta t}{m \times \Delta V} \tag{1}$$

where I is the discharge current (A), Δt is the discharge time (s), ΔV is the voltage change (V) during the discharge process and m is the total mass of the active material. The electrochemical performance of OMC/GA based ASSSs was examined by CV. The interfacial capacitance of electrode based on ASSSs was calculated from the voltammetric responses by summing the charge current in the positive and negative scan directions and dividing the sum by twice the scan rate, according to the following equation:

$$C = \frac{\int I \mathrm{d}V}{2mS\Delta U} \tag{2}$$

where C is denoted as the capacitance contribution from OMC/GAs, GA and OMC electrodes, I is the voltammetric discharge current (A), S is the scan rate (V s^{-1}), ΔU is the absolute value of potential window (V), and m is the total mass of the active material (g). The electrochemical performance of all solid-state devices shown in the Ragone plot was based on the capacitance from Equation 2. The energy density of the device was obtained from the formula given in:

$$E = \frac{1}{2} \times C \times \frac{\Delta V^2}{3{,}600} \tag{3}$$

where E is the energy density (Wh Kg^{-1}), C is the capacitance obtained from Equation 2 and ΔV is the discharge voltage range (V). The power density was calculated from the formula:

$$P = \frac{E}{\Delta t} \times 3600 \tag{4}$$

where P is the power density (W Kg^{-1}), E is the energy density obtained from Equation 3 and Δt is the discharge time (s).

Supporting Information

Supporting Information is available from the Wiley Online Library or from the author.

Acknowledgements

This work was financially supported 973 Program of China (2013CB328804 and 2014CB239701), National Natural Science Foundation of China (21343002, 21102091, 61235007 and 21372155), Program for Professor of Special Appointment (Eastern Scholar) and Program for Innovative Research Team in University (No. IRT13078). The authors also thank Lab for Microstructure, Instrumental Analysis and Research Center, Shanghai University, for materials characterizations.

Received: September 20, 2014
Revised: October 28, 2014

---

[1] a) A. Ambrosi, C. K. Chua, A. Bonanni, M. Pumera, *Chem. Rev.* **2014**, *114*, 7150–7188; b) D. Chen, H. Feng, J. Li, *Chem. Rev.* **2012**, *112*, 6027–6053; c) S. Nardecchia, D. Carriazo, M. Luisa Ferrer, M. C. Gutierrez, F. del Monte, *Chem. Soc. Rev.* **2013**, *42*, 794–830; d) H. Hu, Z. Zhao, W. Wan, Y. Gogotsi, J. Qiu, *Adv. Mater.* **2013**, *25*, 2219–2223; e) M. A. Worsley, P. J. Pauzauskie, T. Y. Olson, J. Biener, J. H. Satcher Jr., T. F. Baumann, *J. Am. Chem. Soc.* **2010**, *132*, 14067–14069; f) L. Qiu, J. Z. Liu, S. L. Y. Chang, Y. Wu, D. Li, *Nat. Commun.* **2012**, *3*, 1241; g) C. Li, G. Shi, *Adv. Mater.* **2014**, *26*, 3992–4012.

[2] a) S. B. Yang, X. L. Feng, K. Müllen, *Adv. Mater.* **2011**, *23*, 3575–3579; b) X. Li, W. Qi, D. Mei, M. L. Sushko, I. Aksay, J. Liu, *Adv. Mater.* **2012**, *24*, 5136–5141; c) D. Wu, F. Zhang, H. Liang, X. Feng, *Chem. Soc. Rev.* **2012**, *41*, 6160–6177; d) Y. Liang, Y. Li, H. Wang, J. Zhou, J. Wang, T. Regier, H. Dai, *Nat. Mater.* **2011**, *10*, 780–786; e) Z. Niu, L. Liu, L. Zhang, Q. Shao, W. Zhou, X. Chen, S. Xie, *Adv. Mater.* **2014**, *26*, 3681–3687; f) Z.-S. Wu, Y. Sun, Y.-Z. Tan, S. Yang, X. Feng, K. Muellen, *J. Am. Chem. Soc.* **2012**, *134*, 19532–19535.

[3] a) Z.-M. Wang, W. Wang, N. Coombs, N. Soheilnia, G. A. Ozin, *ACS Nano* **2010**, *4*, 7437–7450; b) S. B. Yang, X. L. Feng, L. Wang, K. Tang, J. Maier, K. Müllen, *Angew. Chem.* **2010**, *123*, 5451–5455; *Angew. Chem. Int. Ed.* **2010**, *49*, 4795–4799.

[4] a) Y. Zhao, J. Liu, Y. Hu, H. Cheng, C. Hu, C. Jiang, L. Jiang, A. Cao, L. Qu, *Adv. Mater.* **2013**, *25*, 591–595; b) K. Zhang, L. L. Zhang, X. S. Zhao, J. Wu, *Chem. Mater.* **2010**, *22*, 1392–1401; c) J. L. Vickery, A. J. Patil, S. Mann, *Adv. Mater.* **2009**, *21*, 2180–2184.

[5] a) L. Wang, L. Sun, C. Tian, T. Tan, G. Mu, H. Zhang, H. Fu, *RSC Adv.* **2012**, *2*, 8359–8367; b) M. Li, J. Ding, J. Xue, *J. Mater. Chem. A* **2013**, *1*, 7469–7476; c) Y. Zheng, Y. Jiao, J. Chen, J. Liu, J. Liang, A. Du, W. Zhang, Z. Zhu, S. C. Smith, M. Jaroniec, G. Q. Lu, S. Z. Qiao, *J. Am. Chem. Soc.* **2011**, *133*, 20116–20119; d) Y. Q. Sun, C. Li, G. Q. Shi, *J. Mater. Chem.* **2012**, *22*, 12810–12816.

[6] H. Bai, C. Li, G. Shi, *Adv. Mater.* **2011**, *23*, 1089–1115.

[7] a) Y. Wan, Y. Shi, D. Zhao, *Chem. Mater.* **2008**, *20*, 932–945; b) A. Stein, Z. Wang, M. A. Fierke, *Adv. Mater.* **2009**, *21*, 265–293; c) C. Liang, Z. Li, S. Dai, *Angew. Chem.* **2008**, *120*, 3754–3776; *Angew. Chem. Int. Ed. Engl.* **2008**, *47*, 3696–3717; d) Y. Zhai, Y. Dou, D. Zhao, P. F. Fulvio, R. T. Mayes, S. Dai, *Adv. Mater.* **2011**, *23*, 4828–4850.

[8] a) J. Liang, X. Du, C. Gibson, X. W. Du, S. Z. Qiao, *Adv. Mater.* **2013**, *25*, 6226–6231; b) L. L. Zhang, X. S. Zhao, *Chem. Soc. Rev.* **2009**, *38*, 2520–2531; c) P. F. Fulvio, R. T. Mayes, X. Wang, S. M. Mahurin, J. C. Bauer, V. Presser, J. McDonough, Y. Gogotsi, S. Dai, *Adv. Funct. Mater.* **2011**, *21*, 2208–2215.

[9] Y. Xu, K. Sheng, C. Li, G. Shi, *ACS Nano* **2010**, *4*, 4324–4330.

[10] Y. Wan, H. Yang, D. Zhao, *Acc. Chem. Res.* **2006**, *39*, 423–432.

[11] a) Y. Fang, Y. Lv, R. Che, H. Wu, X. Zhang, D. Gu, G. Zheng, D. Zhao, *J. Am. Chem. Soc.*, **2013**, *135*, 1524–1530; b) H. Yang, N. Coombs, I. Sokolov, G. A. Ozin, *Nature* **1996**, *381*, 589–592; c) A. Sellinger, P. M. Weiss, A. Nguyen, Y. F. Lu, R. A. Assink, W. L. Gong, C. J. Brinker, *Nature* **1998**, *394*, 256–260.

[12] Y. Fang, D. Gu, Y. Zou, Z. Wu, F. Li, R. Che, Y. Deng, B. Tu, D. Zhao, *Angew. Chem.* **2010**, *122*, 8159–8163; *Angew. Chem. Int. Ed.* **2010**, *49*, 7987–7991.

[13] D. Zhao, Y. Wan, W. Zhou, *Ordered mesoporous materials*, Wiley-VCH Verlag & Co. KGaA, Weinheim, Germany **2013**.

[14] H. Lu, W. Dai, M. Zheng, N. Li, G. Ji, J. Cao, *J. Power Sources* **2012**, *209*, 243–250.

[15] M. D. Stoller, S. Park, Y. Zhu, J. An, R. S. Ruoff, *Nano Lett.* **2008**, *8*, 3498–3502.

[16] Z.-S. Wu, A. Winter, L. Chen, Y. Sun, A. Turchanin, X. Feng, K. Müllen, *Adv. Mater.* **2012**, *24*, 5130–5135.

[17] a) F. Meng, X. Zhang, B. Xu, S. Yue, H. Guo, Y. Luo, *J. Mater. Chem.* **2011**, *21*, 18537–18539; b) Z. Wang, L. Yue, Z.-T. Liu, Z.-H. Liu, Z. Hao, *J. Mater. Chem.* **2012**, *22*, 14101–14107; c) Y. Qian, I. M. Ismail, A. Stein, *Carbon* **2014**, *68*, 221–231.

[18] a) S. Manne, H. E. Gaub, *Science* **1995**, *270*, 1480–1482; b) S. O. Nielsen, G. Srinivas, C. F. Lopez, M. L. Klein, *Phys. Rev. Lett.* **2005**, *94*.

[19] C.-W. Huang, C.-H. Hsu, P.-L. Kuo, C.-T. Hsieh, H. Teng, *Carbon* **2011**, *49*, 895–903.

[20] Z. S. Wu, K. Parvez, X. Feng, K. Müllen, *Nat. Commun.* **2013**, *4*.

[21] W. S. Hummers, R. E. Offeman, *J. Am. Chem. Soc.* **1958**, *80*, 1339–1339.

[22] J. J. Yoo, K. Balakrishnan, J. Huang, V. Meunier, B. G. Sumpter, A. Srivastava, M. Conway, A. L. Mohana Reddy, J. Yu, R. Vajtai, P. M. Ajayan, *Nano Lett.* **2011**, *11*, 1423–1427.